



Deposited via The University of York.

White Rose Research Online URL for this paper:

<https://eprints.whiterose.ac.uk/id/eprint/142616/>

Version: Accepted Version

---

**Article:**

Decker, Zachary, Zarzana, Kyle J., Coggon, Matthew et al. (2019) Nighttime chemical transformation in biomass burning plumes: A box model analysis initialized with aircraft observations. *Environmental Science and Technology*. pp. 2529-2538. ISSN: 1520-5851

<https://doi.org/10.1021/acs.est.8b05359>

---

**Reuse**

Items deposited in White Rose Research Online are protected by copyright, with all rights reserved unless indicated otherwise. They may be downloaded and/or printed for private study, or other acts as permitted by national copyright laws. The publisher or other rights holders may allow further reproduction and re-use of the full text version. This is indicated by the licence information on the White Rose Research Online record for the item.

**Takedown**

If you consider content in White Rose Research Online to be in breach of UK law, please notify us by emailing [eprints@whiterose.ac.uk](mailto:eprints@whiterose.ac.uk) including the URL of the record and the reason for the withdrawal request.

1 Supporting Information for Nighttime chemical transformation  
2 in biomass burning plumes: a box model analysis initialized  
3 with aircraft observations

4 *Zachary C. J. Decker<sup>1,2,3</sup>, Kyle J. Zarzana<sup>1,2,3</sup>, Matthew Coggon<sup>1,3</sup>, Kyung-Eun Min<sup>1,3,†</sup>, Ilana*  
5 *Pollack<sup>1,††</sup>, Thomas B. Ryerson<sup>3</sup>, Jeff Peischl<sup>1,3</sup>, Pete Edwards<sup>4</sup>, William P. Dubé<sup>1,3</sup>, Milos Z.*  
6 *Markovic<sup>1,†††</sup>, James M. Roberts<sup>1,3</sup>, Patrick R. Veres<sup>3</sup>, Martin Graus<sup>1,††††</sup>, Carsten Warneke<sup>1,3</sup>,*  
7 *Joost de Gouw<sup>1,2</sup>, Lindsay E. Hatch<sup>5</sup>, Kelley C. Barsanti<sup>5</sup>, Steven S. Brown<sup>2,3,\*</sup>*

8 <sup>1</sup>Cooperative Institute for Research in Environmental Sciences, University of Colorado, Boulder,  
9 Colorado, 80309, United States. <sup>2</sup>Department of Chemistry, University of Colorado, Boulder,  
10 Colorado 80309-0215, United States. <sup>3</sup>NOAA Earth System Research Laboratory (ESRL),  
11 Chemical Sciences Division, Boulder, Colorado 80305, United States. <sup>4</sup>Wolfson Atmospheric  
12 Chemistry Laboratories, Department of Chemistry, University of York, York YO10 5DD, United  
13 Kingdom. <sup>5</sup>Department of Chemical and Environmental Engineering and College of  
14 Engineering – Center for Environmental Research and Technology (CE-CERT), University of  
15 California, Riverside, California 92507, United States. <sup>†</sup>Now at Gwangju Institute of Science and  
16 Technology, School of Earth Sciences and Environmental Engineering, Gwangju, South Korea  
17 61005. <sup>††</sup>Now at Colorado State University, Atmospheric Science Department, Ft. Collins, CO,  
18 USA 80523-1371. <sup>†††</sup>Now at Picarro inc, Santa Clara, CA, 95054. <sup>††††</sup>Now at the Department of  
19 Atmospheric and Cryospheric Sciences, University of Innsbruck, Austria 6020.

20 \* steven.s.brown@noaa.gov

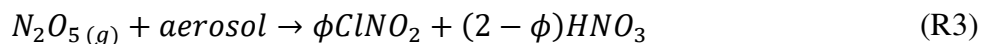
21 Abstract: Biomass burning (BB) is a large source of reactive compounds to the atmosphere. While  
22 the daytime photochemistry of BB emissions has been studied in some detail, there has been little  
23 focus on nighttime reactions despite the potential for substantial oxidative and heterogeneous  
24 chemistry. Here we present the first analysis of nighttime aircraft intercepts of agricultural BB  
25 plumes using observations from the NOAA WP-3D aircraft during the 2013 Southeast Nexus  
26 (SENEX) campaign. We use these observations in conjunction with detailed chemical box  
27 modeling to investigate the formation and fate of oxidants ( $\text{NO}_3$ ,  $\text{N}_2\text{O}_5$ ,  $\text{O}_3$ , and  $\text{OH}$ ) and BB  
28 volatile organic compounds (BBVOCs), using emissions representative of agricultural burns (rice  
29 straw) and western wildfires (ponderosa pine). Field observations suggest  $\text{NO}_3$  production was  
30 approximately  $1 \text{ ppbv hr}^{-1}$ , while  $\text{NO}_3$  and  $\text{N}_2\text{O}_5$  were at or below 3 pptv, indicating rapid  
31  $\text{NO}_3/\text{N}_2\text{O}_5$  reactivity. Model analysis shows that >99% of  $\text{NO}_3/\text{N}_2\text{O}_5$  loss is due to BBVOC +  $\text{NO}_3$   
32 reactions rather than aerosol uptake of  $\text{N}_2\text{O}_5$ . Nighttime BBVOC oxidation for rice straw and  
33 ponderosa pine fires is dominated by  $\text{NO}_3$  (72, 53%, respectively) but  $\text{O}_3$  oxidation is significant  
34 (25, 43%) leading to roughly 55% overnight depletion of the most reactive BBVOCs and  $\text{NO}_2$ .

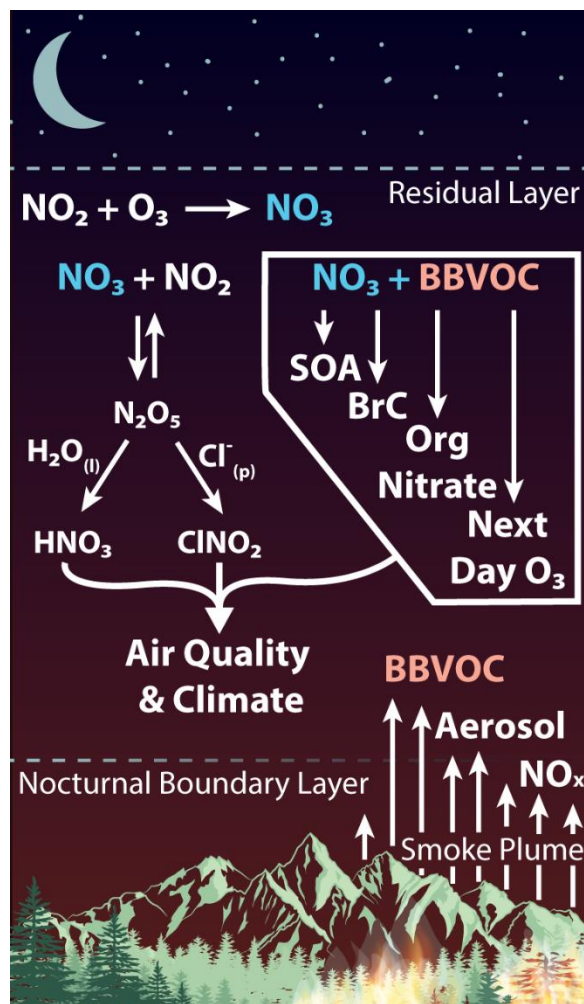
## 35 **Introduction**

36 Wildfire size and frequency in the Western U.S. has increased over the last 20 years, and these  
37 trends are projected to continue due to factors such as forest management practices, elevated  
38 summer temperatures, earlier snowmelt, and drought.<sup>1,2</sup> Biomass burning (BB), including  
39 wildfires, prescribed burning, and agricultural burning, represents a large, imperfectly  
40 characterized and chemically complex source of reactive material to the troposphere. BB releases  
41 reactive species and particulate matter that impact the radiative balance of the atmosphere, air

42 quality, and human health on local to global scales.<sup>3-7</sup> The gas-phase components of BB plumes  
43 include volatile organic compounds (BBVOCs) as well as nitrogen oxides ( $\text{NO}_x = \text{NO} + \text{NO}_2$  and  
44 higher oxides such as peroxyacyl and alkyl nitrates), oxidants, and oxidant precursors. The air  
45 quality and climate effects of BB emissions are defined in part by the oxidative processes and  
46 atmospheric chemical cycles that occur as the smoke is transported, diluted, and exposed to  
47 oxidants over the hours and weeks following emission.

48 The photochemistry of BB plumes has been studied previously in a number of field and  
49 laboratory studies. Daytime BB plumes can have OH concentrations 5-10 times higher than  
50 background air<sup>8</sup> and daytime reactions of  $\text{NO}_x$ , BBVOCs, and OH involve complex pathways  
51 that generally lead to  $\text{O}_3$  formation, but in some cases to near-field  $\text{O}_3$  titration.<sup>9-14</sup> Much less is  
52 known about nighttime BB plume oxidative processes, which are expected to be dominated by  
53 nitrate radicals ( $\text{NO}_3$ ) and  $\text{O}_3$ .<sup>15</sup>  $\text{NO}_3$  is formed by  $\text{O}_3$  oxidation of  $\text{NO}_x$  (R1 & Figure 1) but is  
54 rapidly ( $\tau < 10$  s) destroyed in the daytime by NO and photolysis.<sup>15,16</sup>  $\text{NO}_3$  is a precursor for  
55  $\text{N}_2\text{O}_5$  (R2), a  $\text{NO}_x$  reservoir.  $\text{N}_2\text{O}_5$  may undergo heterogeneous uptake to form  $\text{ClNO}_2$  and  $\text{HNO}_3$   
56 (R3). The former is a daytime Cl radical precursor affecting both marine and continental  
57 environments and influencing next-day  $\text{O}_3$  production.<sup>17-20</sup>  $\text{NO}_3$  can also be directly taken up  
58 onto aerosol (R4).





59  
 60 **Figure 1.** Schematic of nighttime  $\text{NO}_3$  and  $\text{N}_2\text{O}_5$  chemical processing in a biomass burning  
 61 plume.

62 Mixing of background or smoke-derived<sup>14</sup>  $\text{O}_3$  with  $\text{NO}_x$  in a BB plume leads to the production  
 63 of  $\text{NO}_3$ , which may be rapid ( $>0.5$  ppbv  $\text{hr}^{-1}$ ). Recent laboratory measurements conducted during  
 64 both the Fire Lab at Missoula Experiment (FLAME-4) and the on-going Fire Influence on  
 65 Regional and Global Environments Experiment (FIREX) have provided detailed identification  
 66 and quantification of emissions for a range of BBVOCs.<sup>4,5,21–23</sup> Emissions inventories from these  
 67 experiments indicate that the compounds emitted and their relative concentrations depend on the  
 68 fuel type (e.g., pine vs. grass), combustion process (e.g., smoldering or flaming), ignition

69 procedure (fast or slow), and pyrolysis temperature (e.g., high or low).<sup>4,21,24,25</sup> Generally, primary  
70 BBVOC emissions include oxygenated hydrocarbons and aromatics (e.g., phenols), as well as  
71 unsaturated hydrocarbons, biogenic and hetero-aromatic species.<sup>4,5,21</sup> Many such compounds are  
72 very reactive toward  $\text{NO}_3$ <sup>26-33</sup> and may significantly limit its lifetime, promote secondary  
73 organic aerosol formation (SOA)<sup>34,35</sup>, and alter nighttime oxidative budgets.

74 The co-emission of  $\text{NO}_x$ , highly reactive VOCs, and aerosol particles leads to the potential for  
75 significant nighttime chemical transformations. Despite this potential, there has been only one  
76 aircraft campaign to date from which sampling of nighttime biomass burning plumes has been  
77 reported.<sup>36,37</sup> The Southeast Nexus (SENEX) campaign in 2013 included 20 research flights of an  
78 instrumented NOAA WP-3D aircraft and one of the goals was to study the interactions between  
79 anthropogenic and biogenic emissions.<sup>38</sup> A night flight on July 2-3 targeted the emissions and  
80 nighttime chemistry from a power plant plume near the Mississippi river. During this flight the  
81 WP-3D also targeted and intercepted agricultural BB plumes yielding the first airborne study of  
82 nighttime smoke that included  $\text{NO}_3$  and  $\text{N}_2\text{O}_5$  measurements.<sup>36</sup> Even so there has been no  
83 previous analysis of BB  $\text{NO}_3$  chemistry using nighttime aircraft intercepts.

84 Here, we present the first analysis of nighttime smoke oxidation based on aircraft intercepts of  
85 fire plumes using data from this flight. With these observations we initiate a detailed chemical  
86 box model to understand the chemical evolution of oxidants ( $\text{NO}_3$ ,  $\text{N}_2\text{O}_5$ ,  $\text{O}_3$ , and OH) and  
87 BBVOCs over one night (10 hours) using emissions for rice straw to model a generic agricultural  
88 burning plume. We then use this analysis to model nighttime chemistry in western wildfires  
89 using emissions for a ponderosa pine fire.

## 90 **Field and Laboratory Measurements**

91 Field data for this study were taken from multiple instruments deployed on the NOAA WP-3D  
92 aircraft during the SENEX 2013<sup>38</sup> flight on July 2-3, 2013 (20:00-03:00 CDT). Our analysis  
93 utilizes data from the NOAA nitrogen oxide cavity ring-down spectrometer (CRDS) for NO<sub>2</sub>,  
94 NO<sub>3</sub>, N<sub>2</sub>O<sub>5</sub>, and O<sub>3</sub>,<sup>39-42</sup> as well as the NO<sub>y</sub>O<sub>3</sub> chemiluminescence instrument (CL) for NO, NO<sub>2</sub>,  
95 O<sub>3</sub>, and NO<sub>y</sub><sup>43</sup> with 1 Hz acquisition resolution. Within the plume regions we study, the  
96 measurements of NO<sub>2</sub> and O<sub>3</sub> from the CRDS and CL instruments agree within 7%. We also use  
97 data from an ultra-high sensitivity aerosol spectrometer (UHSAS) for aerosol size measurements  
98 (1Hz)<sup>44,45</sup> and a proton-transfer-reaction mass spectrometer (PTR-MS) for VOC measurements  
99 (1 s every 17 s)<sup>46</sup>.

100 BB intercepts were identified by the enhancement above background of four species: black  
101 carbon (BC), glyoxal (CHOCHO), CO, and acryloyl peroxyxynitrate (APAN).<sup>36,47</sup> BB identifier  
102 data were provided by the NOAA airborne cavity enhanced spectrometer (ACES)<sup>48</sup> for glyoxal,  
103 iodide chemical ionization mass spectrometer (I-CIMS) for APAN<sup>49</sup>, single particle soot  
104 photometer (SP2) for black carbon<sup>50</sup>, and vacuum ultra-violet fluorimeter for CO<sup>51</sup>. Power plant  
105 plumes were identified by above background enhancements of NO<sub>x</sub> and N<sub>2</sub>O<sub>5</sub>. While CO is also  
106 present in the power plant plumes, the three other BB identifiers were not. Information on  
107 background and plume measurements are in the SI (Table S1 & S2).

108 Five VOCs (toluene, isoprene + furan, methylvinylketone + methacrolein (MVK+MACR), and  
109 methylethylketone (MEK)) as well as acetonitrile were measured by the PTR-MS during SENEX  
110 and overlap with our inventory. However, we explain in the SI that we do not use these  
111 observations because we do not know the fire source, number of fires, or fuel and plume age  
112 estimates are highly uncertain (Figure S5).

113 Our detailed chemical box model uses emission inventories from Hatch et al.<sup>5</sup> and Koss et al.<sup>4</sup>  
114 for the ponderosa pine and rice straw fuels. The BBVOC emissions from Hatch et al.<sup>5,21</sup> were  
115 measured during FLAME-4 using the following instruments: two-dimensional gas  
116 chromatography–time-of-flight mass spectrometry, open-path Fourier-transform infrared  
117 spectroscopy<sup>22</sup>, whole-air sampling with one-dimensional gas chromatography–mass  
118 spectrometry, and PTR time-of-flight mass spectrometry (PTR-ToF)<sup>52</sup>. BBVOC emissions from  
119 Koss et al.<sup>4</sup> were measured by PTR-ToF during FIREX. Details regarding how the two  
120 inventories were merged is included in the SI. In general, for compounds shared between both  
121 inventories, the emission ratios (E1) agree within an order of magnitude with some exceptions  
122 (Figure S6). We propagate this variability into our model results (SI).

### 123 **Analysis and Modeling Methods**

124 We report our emissions in the form of laboratory-derived emission ratios (ER), which is the  
125 background subtracted emitted compound ( $x$ ) normalized to background subtracted CO.<sup>4,21</sup>

$$ER_x = \frac{x \text{ (ppbv)}}{CO \text{ (ppmv)}} \quad (\text{E1})$$

126 These emissions are integrated over the entirety of the laboratory fires and therefore contain  
127 emissions from all stages of the fire.

128 The modified combustion efficiency (MCE) was calculated for each plume.

$$MCE = \frac{CO_2 - CO_{2bkg}}{(CO_2 - CO_{2bkg}) + (CO - CO_{bkg})} \quad (\text{E2})$$

129 During plume intercepts, the average MCE was  $95 \pm 6\%$ , which is consistent with previous  
130 MCE calculations of the July 2/3 night flight.<sup>36</sup>

131 Total NO<sub>3</sub> reactivity toward BBVOCs is given by

$$k_{NO_3}^{BBVOC} = \sum k_{NO_3+BBVOC_i} [BBVOC_i] \quad (E3)$$

132 where  $k_{NO_3+BBVOC_i}$  is the bimolecular rate coefficient for  $NO_3 + BBVOC_i$  and  $k_{NO_3}^{BBVOC}$  is the  
 133 pseudo-first order rate coefficient. The bimolecular rate coefficients for  $NO_3$ ,  $O_3$ , or  $OH +$   
 134  $BBVOC$  were taken from literature where available and estimated by structure activity  
 135 relationships<sup>31,53</sup> or structural similarity where unavailable (SI).

136 Due to limited literature on  $NO_3 + BBVOC$  rate coefficients, our inventory excludes many  
 137 nitriles, amines, alkynes, acids, and other compounds whose rate coefficients were unavailable  
 138 and could not be estimated. We also removed saturated hydrocarbons because they are generally  
 139 unreactive toward  $NO_3$ .<sup>28</sup> Despite this, our merged inventory retains about 87% of the total  
 140 inventory carbon mass, or 96% by mass, with 235 compounds from Hatch et al.<sup>5</sup> and 171  
 141 compounds from Koss et al.<sup>4</sup> with 103 compounds shared in both inventories for a total of 303  
 142 unique compounds.

143 To calculate the observed  $NO_3$  reactivity during SENEX BB plume intercepts we determined  
 144  $BBVOC$  concentration using background corrected  $CO$  measured on the WP-3D.

$$BBVOC (ppbv) = ER_{BBVOC} (CO - CO_{bkg}) \quad (E4)$$

145 As shown below,  $BBVOC$  is likely the main sink of  $NO_3$ ; therefore, the extent of  $BBVOC$   
 146 oxidation by  $NO_3$  will be limited by the  $NO_x/BBVOC$  ratio as  $NO_x$  is the source for  $NO_3$  (R1).  
 147 Furthermore, the relative oxidative importance between  $O_3$  and  $NO_3$  depends on the  
 148  $NO_x/BBVOC$  ratio as explained by Edwards et al.<sup>54</sup> Therefore, in contrast to the method used for  
 149 calculating  $BBVOC$  concentration in SENEX fire plume intercepts described above, we initiate  
 150 our box model with fire emissions scaled to  $NO_x$  in order to preserve the  $NO_x/VOC$  ratio  
 151 observed during the fire lab experiments.

152 To estimate the emitted  $\text{NO}_x$  at the fire source we assume that the total reactive nitrogen ( $\text{NO}_y$ ,  
153 which does not include  $\text{NH}_3$ ) is equivalent to the emitted  $\text{NO}_x$ . The  $\text{NO}_x/\text{NO}_y$  ratio as measured  
154 during SENEX fire plume intercepts in Figure 2 was 0.84. We calculated the observed  $\text{NO}_y$   
155 emission ratio using  $\text{NO}_y$  ( $13.2 \pm 3.1$  ppbv) and CO ( $543.4 \pm 87.7$  ppbv) enhancements above  
156 background. The calculated  $\text{NO}_y$  emission ratio, which we assume to be the  $\text{NO}_x$  emission ratio  
157 at the fire source, was determined to be  $24.3 \pm 6.4$  ppbv  $\text{NO}_y/\text{ppmv CO}$  for the plume intercept.  
158 We compared the estimated observed  $\text{NO}_x$  emission ratio to the  $\text{NO}_x$  emission ratios reported by  
159 Selimovic et al. for rice straw ( $43.9$  ppbv  $\text{NO}_x/\text{ppmv CO}$ ) and ponderosa pine ( $26.9 \pm 4.3$  ppbv  
160  $\text{NO}_x/\text{ppmv CO}$ ).<sup>23</sup> We then scaled the BBVOC emissions by this ratio (E5), effectively scaling  
161 the fire emissions to the  $\text{NO}_x$  of the observed fire plume.

$$[BBVOC]^{model} = [BBVOC]^{inventory} * \frac{ER_{NO_y}^{observed}}{ER_{NO_x}^{inventory}} \quad (E5)$$

162 The  $\text{NO}_x$  emission ratio observed during the SENEX fire plume intercepts in Figure 2 was 45%  
163 and 11% lower than the laboratory-derived  $\text{NO}_x$  emission ratio for rice straw and ponderosa pine  
164 fires respectively. To correctly model the  $\text{NO}_3$  oxidation of these fires we reduced our BBVOC  
165 emissions by a factor of 55% for rice straw and 89% for ponderosa pine.

166 Model background and initial concentrations of  $\text{NO}_x$ , CO, and  $\text{O}_3$  were taken from the SENEX  
167 observations shown in Figure 2. We estimate the  $\text{NO}/\text{NO}_2$  ratio at the fire source using the NO  
168 and  $\text{NO}_2$  emission ratios from FIREX for each fuel. The  $\text{NO}/\text{NO}_2$  ratios used are 5.3 and 2.8 for  
169 rice straw and ponderosa pine, respectively.<sup>23</sup> The background  $\text{NO}_2$  mixing ratio was taken to be  
170 0.9 ppbv. The background  $\text{O}_3$  mixing ratio, 43.9 ppbv, was used as the starting  $\text{O}_3$  mixing ratio  
171 and is representative of the background  $\text{O}_3$  in the region where BB plumes were intercepted  
172 (Figure S3).

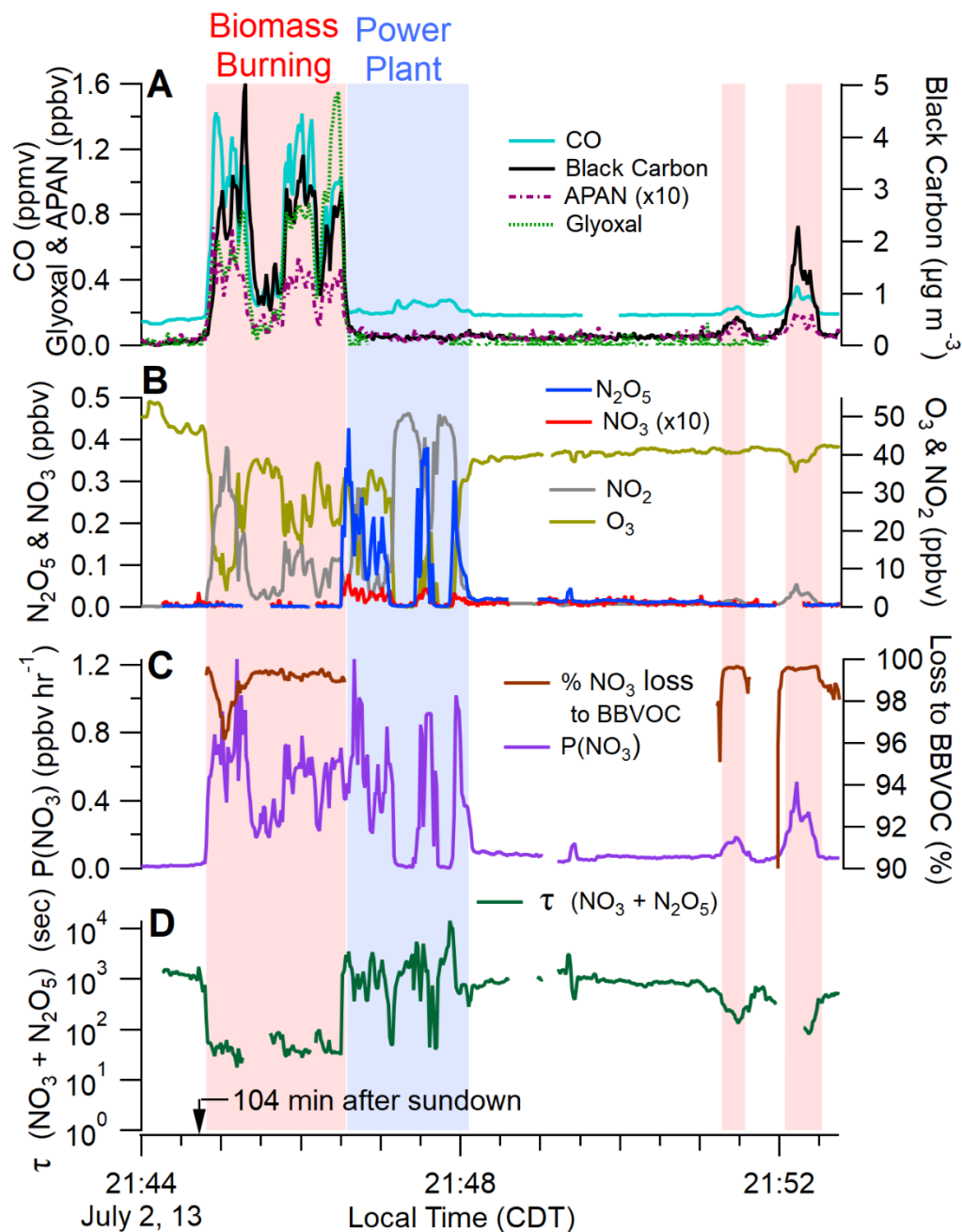
173 Box modeling was performed using the Framework for 0-D Atmospheric Modeling (F0AM)<sup>55</sup>  
174 to investigate the evolution of oxidized mass and oxidant fractions over 10 hours (the  
175 approximate duration of one night in July in the Southeastern U.S.). Chemical mechanisms were  
176 adopted from the MCM (v3.3.1<sup>56-60</sup>, via website: <http://mcm.york.ac.uk>) and published  
177 mechanisms for methylguaiacol, syringol, *o*-guaiacol, and 3-methylfuran were added (Table  
178 S4).<sup>61-63</sup> Compounds not included in the above references were modeled as a one-step reaction of  
179 BBVOC + NO<sub>3</sub>, BBVOC + O<sub>3</sub>, or BBVOC + OH to form a single oxidation product.

180 All models were run at 298 K, typical experimental conditions for most published rate  
181 coefficients. Temperatures during flight ranged between 288-290 K (SI). In order to account for  
182 dilution processes, as well as entrainment of O<sub>3</sub>, we apply a first order dilution of  $k_{\text{dil}} = 1.16 \times 10^{-5}$   
183 s<sup>-1</sup>, or a 24 hour lifetime. The sensitivity of this assumption is shown in Figure S2 and discussed  
184 in the SI. We report a base case model result with upper and lower bound uncertainties based on  
185 the emission and rate coefficient uncertainties. Although, as discussed in the SI, the bounds do  
186 not provide information on the error distribution.

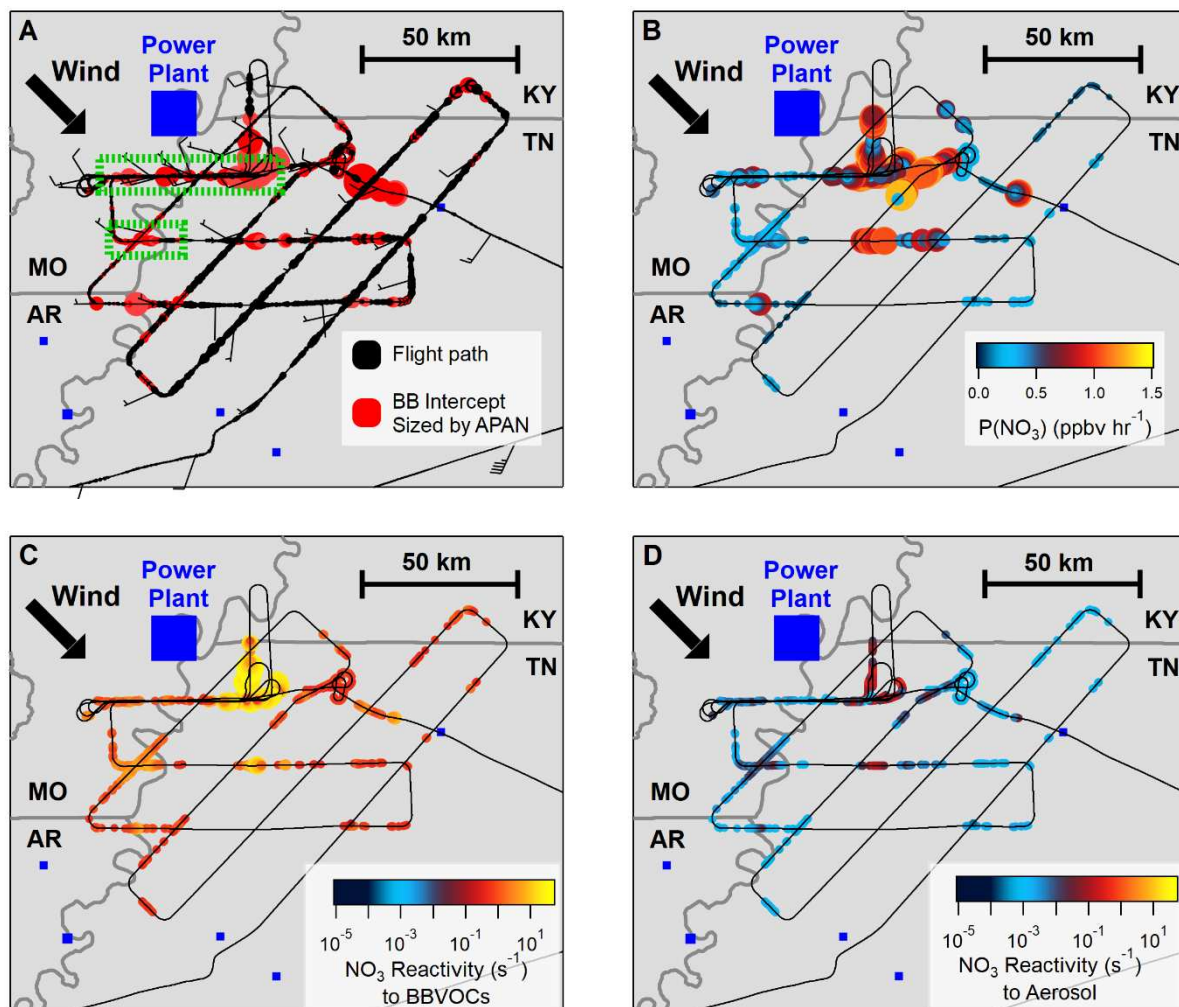
## 187 **Results and Discussion**

188 In panel A of Figure 2 the power plant plume intercepts (blue background) are distinguished  
189 from the fire plume intercepts (red background) by CO, black carbon, APAN, and glyoxal.  
190 Intercepts shown in Figure 2 were at an altitude between 700-900 meters. Relative to the BB  
191 plume intercepts, the power plant plume intercepts exhibited elevated levels of NO<sub>3</sub> and N<sub>2</sub>O<sub>5</sub>  
192 (Figure 2B). Figure 3A shows a flight map of the July 2-3 flight colored red during BB plume  
193 intercepts and sized by the APAN mixing ratio. Roughly 97% of the indicated BB plumes do not  
194 show signs of power plant plume mixing (SI). Green dashed boxes indicate sections of data  
195 shown in Figure 2.

196 The flight covered the intersection of Missouri, Kentucky, Tennessee, and Arkansas at the  
197 Mississippi river. According to the USDA CropScape database, this land is mainly agricultural  
198 and therefore the fire plume is most likely the result of burning crop residue and stubble.<sup>36,64</sup>  
199 Plume intercepts occurred near winter wheat crops, and rice straw crops are situated roughly 70  
200 km northwest. Still, rice straw is the best available fuel proxy for agricultural burning emissions.  
201 The wind direction was roughly northwesterly with most BB plume intercepts occurring in the  
202 northwest corner of Tennessee.



203  
 204 **Figure 2.** Time traces during representative sections of BB (red) and power plant (blue) plume  
 205 intercepts made 104 minutes after sundown ( $\text{SZA}=90^\circ$ ). A: BB tracers, B:  $\text{NO}_3$ ,  $\text{N}_2\text{O}_5$ ,  $\text{NO}_2$ , and  
 206  $\text{O}_3$  mixing ratio, C: production rate of  $\text{NO}_3$  and the percentage of  $\text{NO}_3$  reactivity toward  
 207 BBVOCs, D: lifetime of  $\text{NO}_3$  and  $\text{N}_2\text{O}_5$ .



208 **Figure 3.** Flight maps of the SENEX July 2-3 2013 night flight. A: BB intercepts colored by red  
 209 markers, sized by APAN (0.01-0.1 ppbv), and green dashes indicate sections shown in Figure 2,  
 210 B: Production rate of NO<sub>3</sub>, C: and D: are comparisons of NO<sub>3</sub> reactivity toward BBVOCs (C)  
 211 and toward aerosol (D) on the same color and log scale.

212 To illustrate the NO<sub>3</sub> chemistry within a BB plume, we use previously published NO<sub>3</sub> and  
 213 N<sub>2</sub>O<sub>5</sub> analysis metrics. The NO<sub>3</sub> production rate, P(NO<sub>3</sub>), is the instantaneous source of NO<sub>3</sub>  
 214 from the reaction of NO<sub>2</sub> with O<sub>3</sub> and is given in (E6).<sup>15</sup> The NO<sub>3</sub> + N<sub>2</sub>O<sub>5</sub> lifetime ( $\tau$ ) is the ratio  
 215 of NO<sub>3</sub> and N<sub>2</sub>O<sub>5</sub> concentration to the NO<sub>3</sub> production rate (E7).<sup>65</sup> The summed lifetime is useful

216 because  $\text{NO}_3$  and  $\text{N}_2\text{O}_5$  reach an equilibrium state that is typically more rapid than the individual  
217 sink reactions for either, such that they can be regarded as a sum.

$$P(\text{NO}_3) = k_{\text{NO}_3}[\text{NO}_2][\text{O}_3] \quad (\text{E6})$$

$$\tau(\text{NO}_3 + \text{N}_2\text{O}_5) = \frac{\text{NO}_3 + \text{N}_2\text{O}_5}{P(\text{NO}_3)} \quad (\text{E7})$$

218  $P(\text{NO}_3)$  was large and of similar magnitude in both the power plant plume and BB plume  
219 (Figure 2C). Figure 3B is colored by  $\text{NO}_3$  production during BB intercepts only, and shows that  
220 large  $\text{NO}_3$  production rates, near  $1 \text{ ppbv hr}^{-1}$ , were observed during multiple BB plume  
221 intercepts. Despite the large  $\text{NO}_3$  radical production, the  $\text{NO}_3$  and  $\text{N}_2\text{O}_5$  concentrations within the  
222 BB plume were below the  $3 \text{ pptv}^{38}$  stated detection limit of the instrument (Figure 2B), yielding  
223 short  $\text{NO}_3 + \text{N}_2\text{O}_5$  lifetimes. Indeed, as shown in Figure 2D,  $\tau$  is roughly a factor of 100 lower  
224 within the BB plume as compared to the power plant plume and background air. Because the  
225  $\text{NO}_3$  and  $\text{N}_2\text{O}_5$  were below stated detection limits in the BB plumes, the corresponding lifetimes  
226 shown in Figure 2D are upper limits, and the actual lifetimes may be considerably shorter.

227 The high production rate and short lifetime of  $\text{NO}_3 + \text{N}_2\text{O}_5$  within the BB plume is evidence  
228 for rapid  $\text{NO}_3$  or  $\text{N}_2\text{O}_5$  loss pathways. BB plumes contain large quantities of both aerosol and  
229 BBVOCs, which provide two efficient  $\text{NO}_3/\text{N}_2\text{O}_5$  loss pathways. To understand the competition  
230 between these loss processes we calculated an instantaneous  $\text{NO}_3$  reactivity toward aerosol and  
231 toward BBVOCs. The total  $\text{NO}_3$  loss to BBVOC is calculated using the sum of BBVOC  
232 reactivity normalized to CO (E3). The total  $\text{NO}_3$  loss to aerosol uptake is given as the sum of  
233 both  $\text{NO}_3$  and  $\text{N}_2\text{O}_5$  uptake rate coefficients. By assuming steady state<sup>66</sup> for both  $\text{NO}_3$  and  $\text{N}_2\text{O}_5$ ,  
234 we estimate the total aerosol uptake, and therefore  $\text{NO}_3$  reactivity toward aerosol, as

$$k_{\text{NO}_3}^{\text{aerosol}} = K_{\text{eq}}[\text{NO}_2]k_{\text{N}_2\text{O}_5+\text{aerosol}} + k_{\text{NO}_3+\text{aerosol}} \quad (\text{E8})$$

235 where  $k_{NO_3}^{aerosol}$  is a first order rate coefficient,  $K_{eq}$  is the equilibrium constant between  $NO_3$  and  
236  $N_2O_5$  (R2), and  $k_{x+aerosol}$  is the first order rate coefficient for  $N_2O_5$  or  $NO_3$  aerosol uptake  
237 expressed below.

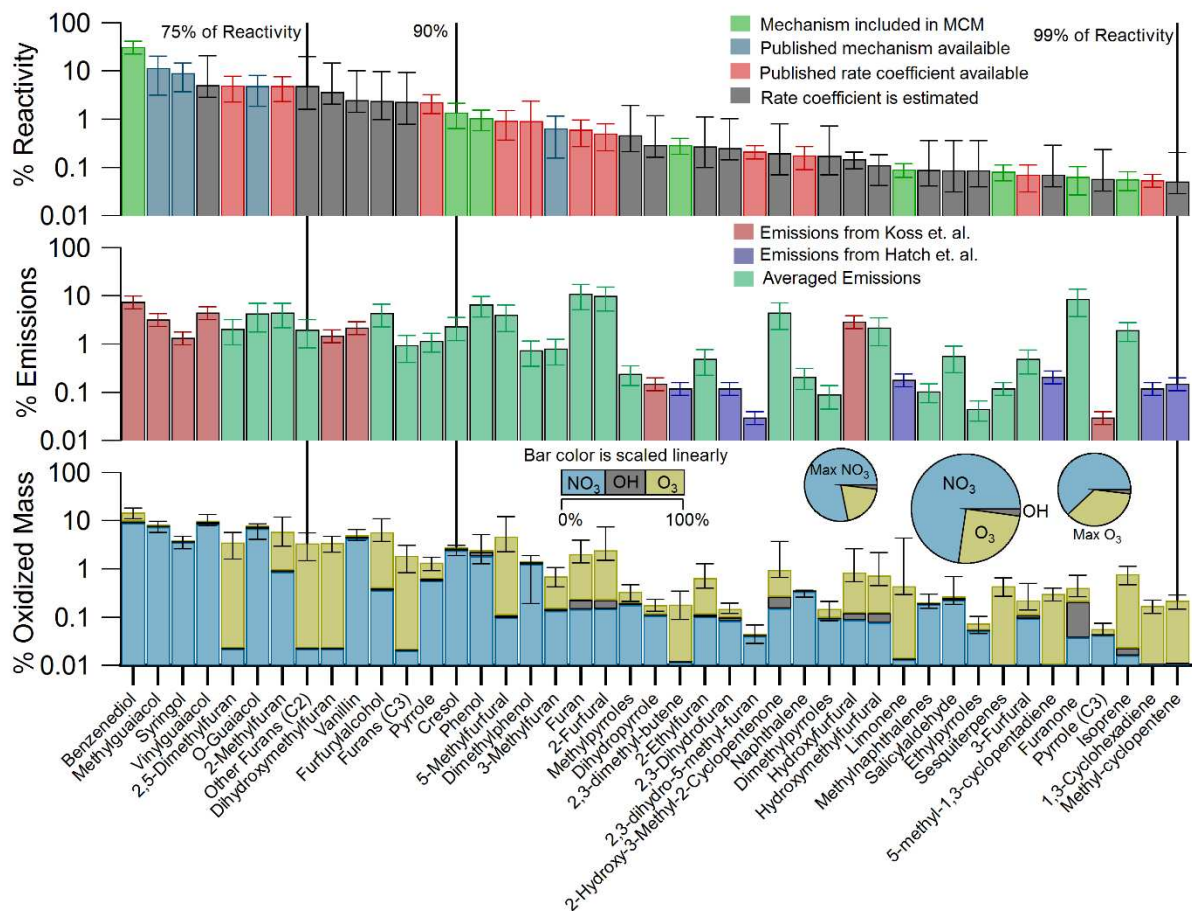
$$k_{x+aerosol} = \frac{\gamma \cdot \bar{c} \cdot SA}{4} \quad (E9)$$

238 Here,  $\gamma$  is the aerosol uptake coefficient,  $\bar{c}$  is the mean molecular speed, and SA is the aerosol  
239 surface area. Calculations use uptake coefficients of  $\gamma_{N_2O_5} = 10^{-2}$  for  $N_2O_5$ <sup>19</sup> and  $\gamma_{NO_3} = 10^{-3}$   
240 for  $NO_3$ . However,  $\gamma_{NO_3}$  values have a wide range therefore we include calculations with  $\gamma_{NO_3} =$   
241 1 in the SI, but find similar results.<sup>15</sup>

242 Figure 3C & D compare the  $NO_3$  reactivity toward BBVOCs, and aerosol uptake during BB  
243 plume intercepts, respectively. In all BB intercepts, the calculated  $NO_3$  reactivity toward  
244 BBVOCs is a factor of 100 - 1000 greater than aerosol uptake. Figure 2C shows the percentage  
245 of  $NO_3$  reactivity dominated by BBVOC with a median >99%.

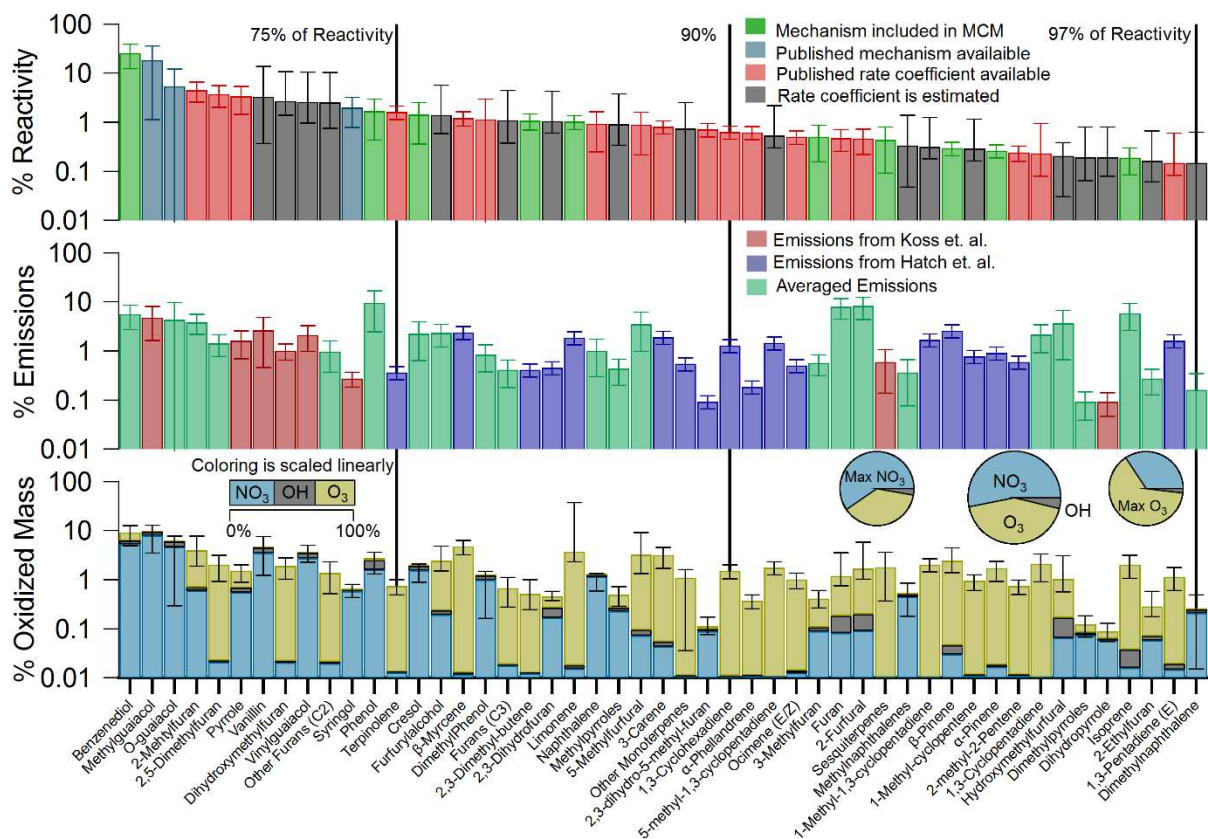
246 To understand which BBVOCs may be responsible for the rapid initial loss of  $NO_3$  we  
247 calculated the relative  $NO_3$  reactivity for 303 compounds in rice straw and ponderosa pine  
248 burning emissions. The top panel of Figure 4 shows the ranked order of the compounds that  
249 account for 99% of the rice straw initial  $NO_3$  reactivity. Eight furan or phenol compounds are  
250 responsible for 75% of the initial  $NO_3$  reactivity. Most of, the initial  $NO_3$  reactivity for a rice  
251 straw fire is accounted for by phenols ( $60_{-14}^{+20}\%$ ) and furans ( $23_{-6}^{+20}\%$ ), as well as pyrroles and  
252 furfurals ( $8_{-3}^{+9}\%$  combined).

253



254  
 255 **Figure 4.** Rice Straw fuel. The top panel shows the ranked order of the compounds that account  
 256 for 99% of the rice straw initial NO<sub>3</sub> reactivity. The color scale describes the origin of the  
 257 mechanisms or rate coefficient used. The middle panel is the relative BBVOC emission ratio  
 258 normalized to the total BBVOC emission ratio and the color scale describes the origin of the  
 259 emissions data. The bottom panel is the relative nighttime reacted mass (10 hours) normalized to  
 260 total reacted mass. While the bar height is on a log scale, the color scale is linear and indicates  
 261 the fraction of oxidation by NO<sub>3</sub> (blue), O<sub>3</sub> (gold), and OH (grey). The center pie chart shows the  
 262 fraction of reacted mass in the base case with the maximum NO<sub>3</sub> oxidation case to the left, and  
 263 maximum O<sub>3</sub> oxidation case to the right. All panels sum to 100%.

264 The top panel of Figure 5 shows the ranked order of the compounds that account for 97% of  
 265 the ponderosa pine initial NO<sub>3</sub> reactivity. The top 75% of initial NO<sub>3</sub> reactivity is distributed  
 266 among 13 compounds with phenols (62<sup>+27</sup><sub>-23</sub>%), furans (18<sup>+12</sup><sub>-4</sub>%), pyrrole and furfural (8<sup>+8</sup><sub>-3</sub>%  
 267 combined) again dominating the total reactivity. Unlike rice straw, a ponderosa pine fire plume  
 268 has significant reactivity towards terpenes (8<sup>+2</sup><sub>-1</sub>%). The initial NO<sub>3</sub> reactivity towards terpenes  
 269 and unsaturated hydrocarbons in a rice straw plume is <1%. These differences in reactivity are  
 270 due to differences in emissions between the two fuels as explained below.<sup>5</sup>



271  
 272 **Figure 5.** Same as Figure 4, but for the ponderosa pine fuel. In the bottom panel the bar height is  
 273 on a log scale, but the color scale is linear and indicates the fraction of oxidation by NO<sub>3</sub> (blue),  
 274 O<sub>3</sub> (gold), and OH (grey).

275 The middle panels of Figures 4 and 5 show the emission ratios for each compound normalized  
276 to total emissions. The color indicates the origin of the emission ratio. The rice straw fire  
277 emissions for compounds included in Figure 4 are mainly furans ( $33\pm 8\%$ ), phenols ( $27\pm 4\%$ ),  
278 and furfurals ( $24\pm 6\%$ ), while unsaturated hydrocarbon and terpene emissions account for only  
279  $3\pm 1\%$ . In contrast, the ponderosa pine fire emissions have a larger representation of terpenes  
280 ( $18\pm 4\%$ ) and unsaturated hydrocarbons ( $10\pm 2\%$ ), but phenols ( $33\pm 10\%$ ), furans ( $17\pm 4\%$ ) and  
281 furfurals ( $18\pm 6\%$ ) are all still significant.

282 To better understand smoke plume evolution and to determine the amount of BBVOC mass  
283 oxidized during one night (10 hours), we ran a 0-D box model for both rice straw and ponderosa  
284 pine fire emissions.  $\text{NO}_3$  and  $\text{N}_2\text{O}_5$  remained below 3 pptv (Figure S1), consistent with field  
285 observations (Figure 2B). Figure S1 illustrates that the summed concentrations of the most  
286 reactive BBVOCs are comparable to  $\text{NO}_2$ , suggesting there is approximately as much  $\text{NO}_3$   
287 precursor available as there is BBVOC to be oxidized. For both fuels, roughly 50-60% of  $\text{NO}_2$   
288 and the BBVOC compounds listed in Figure 4 and Figure 5 are depleted by chemistry (excluding  
289 dilution) in one night. Our box-model suggests several abundant BBVOCs survive the night with  
290 more than 50% of their initial starting concentration, such as phenol, furan, furfural and  
291 hydroxymethylfurfural (SI).

292  $\text{HNO}_3$  production is complex within the model, and both maximum and minimum uncertainty  
293 bounds on  $\text{HNO}_3$  concentrations are the result of higher bound BBVOC emissions, but lower and  
294 higher bound BBVOC rate coefficients, respectively.  $\text{HNO}_3$  is the product of reactions of  
295 phenolic compounds with  $\text{NO}_3$ , which proceeds by H-abstraction.  $\text{HNO}_3$  production is  
296 dominated by catechol +  $\text{NO}_3$  ( $\sim 60\%$ ) within the first few hours, but as the more reactive  
297 compounds are depleted, the lesser reactive compounds like methyl guaiacol, guaiacol and

298 syringol react with  $\text{NO}_3$  and dominate in the last two hours.  $\text{HNO}_3$  may be lost to the particle  
299 phase with concurrent  $\text{NH}_3$  emission or other nitrogen species, however this loss mechanism is  
300 not included in our model.

301 For both fuels, catechol is the most reactive compound, and accounts for  $32\pm 9\%$  and  $26\pm 13\%$   
302 of initial  $\text{NO}_3$  reactivity at the start of the simulation for rice straw and ponderosa pine plumes,  
303 respectively. However, Koss et al.<sup>4</sup> were unable to distinguish between catechol and  
304 methylfurfural at  $m/z = 110.1$ . We assume a 50/50 contribution here, which yields catechol  
305 emission ratios of  $2.5\pm 0.8$  ppbv ppmv<sup>-1</sup> CO for rice straw and  $1.5\pm 0.6$  ppbv ppmv<sup>-1</sup> CO for  
306 ponderosa pine. Still, the high reactivity is mainly due to the large catechol rate coefficient  
307 ( $9.9\cdot 10^{-11}$  cm<sup>3</sup> molecule<sup>-1</sup> s<sup>-1</sup>)<sup>67</sup>, which is the third greatest among the emitted compounds.  
308 Catechol is known to react with  $\text{NO}_3$  by H-abstraction, with subsequent addition of  $\text{NO}_2$  to the  
309 aromatic peroxy radical to form 4-nitrocatechol with a near-unity molar yield of  $0.91\pm 0.06$ .<sup>68</sup>  
310 Further, 4-nitrocatechol is expected to almost completely (96%) partition to the particle phase.<sup>68</sup>  
311 Recently, Hartikainen et al.<sup>25</sup> investigated dark oxidation of residential wood combustion and  
312 found strong correlations between the depletion of phenolic compounds and the formation of  
313  $\text{NO}_3$ -initiated SOA. In wintertime BB events, 4-nitrocatechol and other derivatives have been  
314 detected in aerosol and are considered important light-absorbing components of brown carbon  
315 (BrC).<sup>35,69-76</sup>

316 SOA yields are a function of mass loadings.<sup>77</sup> Using a catechol mass loading of  $300 \mu\text{g m}^{-3}$   
317 from Finewax et al.<sup>68</sup> as well as a total observed aerosol plume measurement of  $58.7 \mu\text{g m}^{-3}$  we  
318 estimate a 4-nitrocatechol SOA mass yield of 120%. Assuming 0.6 ppbv of catechol in  
319 ponderosa pine and 0.8 ppbv in rice straw (initial model conditions) with 44 ppbv  $\text{O}_3$ , 13 ppbv of  
320  $\text{NO}_x$  and  $k_{\text{dil}} = 1.16\cdot 10^{-5}$  s<sup>-1</sup>, we estimate the SOA produced from catechol to be  $3.8\pm 1.0 \mu\text{g m}^{-3}$

321 in 8 hours and  $4.0_{-1.0}^{+1.1} \mu\text{g m}^{-3}$  in 8.5 hours for a rice straw and ponderosa pine plume,  
322 respectively. Further, there is evidence to suggest furans and furfurals may also be a source of  
323 SOA precursors.<sup>5,25</sup>

324 The bottom panel of Figure 4 shows the reacted mass per compound normalized to the total  
325 reacted mass. The bar height is on a log scale, but the bar color is linearly scaled and indicates  
326 the fraction of nighttime oxidation by  $\text{NO}_3$  (blue),  $\text{O}_3$  (gold), and OH (grey) after 10 hours for  
327 each compound. The center pie chart in Figure 4 and 5 represents the base case fraction of  
328 reactant mass oxidized by each oxidant. The left and right pie charts show results for the  
329 estimated maximum possible  $\text{NO}_3$  and maximum possible  $\text{O}_3$  oxidation, respectively.  
330 Uncertainty in the fraction of oxidized mass is calculated from the uncertainties in individual  
331 compound emissions and rate coefficients. For the compounds comprising a rice straw BB  
332 plume, the majority of mass is oxidized by  $\text{NO}_3$  ( $72_{-11}^{+6}\%$ ). This is expected because the rice  
333 straw fuel emissions are rich in oxygenated aromatic and hetero-aromatic emissions, which are  
334 generally less reactive toward  $\text{O}_3$ . Terpenes and unsaturated hydrocarbons, which are a small  
335 fraction of emissions in Figure 4, are relatively more reactive toward  $\text{O}_3$ . Even so,  $\text{O}_3$  still has a  
336 significant oxidative impact and is responsible for  $26_{-6}^{+11}\%$  of oxidized BBVOC mass.

337 The relative amount of oxidized mass for ponderosa pine is shown in the bottom panel of  
338 Figure 5. Almost half of the oxidized mass for compounds included in Figure 5 is due to  $\text{O}_3$   
339 ( $43_{-6}^{+21}\%$ ) for our base case. The phenolic compounds mainly undergo  $\text{NO}_3$  oxidation while  
340 terpenes and unsaturated hydrocarbons are mainly oxidized by  $\text{O}_3$ . Furans and the hetero-  
341 aromatics are oxidized approximately evenly by  $\text{O}_3$  and  $\text{NO}_3$ . The increased fraction of  $\text{O}_3$   
342 oxidation is the result of the increased fraction of unsaturated hydrocarbon and terpenes in the  
343 ponderosa pine emissions when compared to rice straw.

344 The nighttime chemical evolution and oxidation products of a biomass burning plume will  
345 depend on the relative  $\text{NO}_3$  and  $\text{O}_3$  reactivity. Neglecting the small contribution from OH  
346 oxidation, Edwards et al.<sup>54</sup> show the competition between  $\text{NO}_3$  and  $\text{O}_3$  oxidation of biogenic  
347 VOCs (BVOC) is dependent on the  $\text{NO}_x/\text{BVOC}$  ratio. We scaled our BBVOC emissions to  
348 maintain the  $\text{NO}_x/\text{BBVOC}$  ratio expected for rice straw ( $0.4 \pm 0.1$ ) or ponderosa pine ( $0.3 \pm 0.1$ )  
349 emissions. However, because fires are highly variable, the  $\text{NO}_x/\text{BBVOC}$  ratio for any given fuel  
350 may vary from fire to fire. For rice straw, a factor of two increase in  $\text{NO}_x$  increases the fraction  
351 of  $\text{NO}_3$  oxidation from 72% to 84%, while a factor of two decrease in  $\text{NO}_x$  decreases relative  
352  $\text{NO}_3$  oxidation to 55%. Similarly, for ponderosa pine, doubling  $\text{NO}_x$  increases the fraction of  $\text{NO}_3$   
353 oxidation from 53% to 66%, while halving  $\text{NO}_x$  decreases relative  $\text{NO}_3$  oxidation to 37% and  
354 increases  $\text{O}_3$  to 57%. Furthermore, we find that a factor of two change in ambient  $\text{O}_3$   
355 concentration has little effect on the relative  $\text{NO}_3$  and  $\text{O}_3$  reactivity (see SI).

356 Our reactivity calculations and box-model results are most limited by a lack of kinetic and  
357 mechanistic studies for  $\text{O}_3$ ,  $\text{NO}_3$ , and OH + BBVOCs reactions. Kinetic and mechanistic studies  
358 of furan, furfural, phenol, and pyrrole analogues reacting with  $\text{NO}_3$  will be most critical to  
359 understanding nighttime BB processes, which we highlight in the SI.

360 The time of day in which a fire is active will determine the fate of its emissions. This paper  
361 presents the first nighttime aircraft intercepts of a BB plume combined with an inventory of 303  
362 BBVOC emissions and an oxidation model to predict the lifetime and fate of BB emissions in the  
363 dark. Fire emissions at times near sunset will undergo the chemistry we have detailed here,  
364 which suggests a roughly 60% depletion (for both rice straw and ponderosa pine) of fire-derived  
365  $\text{NO}_x$ . We find that nighttime chemistry is likely to proceed by  $\text{NO}_3$ , rather than  $\text{N}_2\text{O}_5$ , further  
366 slowing the loss of  $\text{NO}_x$  (R1 & R2). Our model applies to chemistry at the center of a plume and

367 does not include dispersion. Dispersion mixes  $\text{NO}_x$  with background  $\text{O}_3$  at the edges of the plume  
368 leading to faster depletion, and therefore the values we report are likely lower limits. Even so,  
369 18-19% of BBVOC mass, out of the total BBVOC mass that we model, will be oxidized in one  
370 night. That is roughly a 55% depletion of the BBVOCs that are reactive toward  $\text{NO}_3$ . There is  
371 evidence that many of these  $\text{NO}_3$  reactive compounds can form secondary BrC aerosol<sup>35,69-76</sup>,  
372 suggesting nighttime oxidation may be a significant source of BB derived BrC. Furthermore,  
373 future BB photochemical models should consider that these reactive phenolic-, furan- and  
374 furfural-like compounds are not only reactive toward  $\text{NO}_3$ , but also  $\text{O}_3$  and OH, thus affecting  
375 next-day BB photochemistry.

#### 376 Acknowledgments

377 We'd like to thank Charles A. Brock for aerosol surface area measurements.

#### 378 Supporting Information Available

379 Figure S1, box model time traces of key species, Figure S2, box model sensitivity to the dilution  
380 rate coefficient, Figure S3, Correlation of  $\text{O}_3$  and  $\text{NO}_2$  from aircraft observations, Figure S4,  
381 altitude profiles of key species and potential temperature, Figure S5, plume age estimates, Figure  
382 S6, variability in emission ratios. Table S1, BB plume and background values, Table S2, Plumes  
383 and background times, Table S3, List of reactions excluded from the MCM, Table S4,  
384 mechanisms added to the MCM. This information is available free of charge via the Internet at  
385 <http://pubs.acs.org>.

#### 386 References

387 (1) Dennison, P. E.; Brewer, S. C.; Arnold, J. D.; Moritz, M. A. Large Wildfire Trends in the  
388 Western United States, 1984-2011. *Geophys. Res. Lett.* **2014**, *41*, 2014GL059576.

389 <https://doi.org/10.1002/2014gl059576>.

390 (2) Westerling, A. L.; Hidalgo, H. G.; Cayan, D. R.; Swetnam, T. W. Warming and Earlier  
391 Spring Increase Western U.S. Forest Wildfire Activity. *Science* (80-. ). **2006**, *313* (5789),  
392 940–943.

393 (3) Pope, C. A.; Dockery, D. W. Health Effects of Fine Particulate Air Pollution: Lines That  
394 Connect. *J. Air Waste Manag. Assoc.* **2006**, *56* (6), 709–742.  
395 <https://doi.org/10.1080/10473289.2006.10464485>.

396 (4) Koss, A. R.; Sekimoto, K.; Gilman, J. B.; Selimovic, V.; Coggon, M. M.; Zarzana, K. J.;  
397 Yuan, B.; Lerner, B. M.; Brown, S. S.; Jimenez, J. L.; Krechmer, J.; Roberts, J. M.;  
398 Warneke, C.; Yokelson, R. J.; de Gouw, J. Non-Methane Organic Gas Emissions from  
399 Biomass Burning: Identification, Quantification, and Emission Factors from PTR-ToF  
400 during the FIREX 2016 Laboratory Experiment. *Atmos. Chem. Phys.* **2018**, *18* (October),  
401 3299–3319. <https://doi.org/10.5194/acp-2017-924>.

402 (5) Hatch, L. E.; Yokelson, R. J.; Stockwell, C. E.; Veres, P. R.; Simpson, I. J.; Blake, D. R.;  
403 Orlando, J. J.; Barsanti, K. C. Multi-Instrument Comparison and Compilation of Non-  
404 Methane Organic Gas Emissions from Biomass Burning and Implications for Smoke-  
405 Derived Secondary Organic Aerosol Precursors. *Atmos. Chem. Phys.* **2017**, *17* (2), 1471–  
406 1489. <https://doi.org/10.5194/acp-17-1471-2017>.

407 (6) Rotstayn, L. D.; Penner, J. E. Indirect Aerosol Forcing, Quasi Forcing, and Climate  
408 Response. *J. Clim.* **2001**, *14* (13), 2960–2975. [https://doi.org/10.1175/1520-](https://doi.org/10.1175/1520-0442(2001)014<2960:IAFQFA>2.0.CO;2)  
409 [0442\(2001\)014<2960:IAFQFA>2.0.CO;2](https://doi.org/10.1175/1520-0442(2001)014<2960:IAFQFA>2.0.CO;2).

410 (7) Andreae, M. O.; Merlet, P. Emission of Trace Gases and Aerosols from Biomass Burning.

- 411 *Global Biogeochem. Cycles* **2001**, *15* (4), 955–966.  
412 <https://doi.org/10.1029/2000GB001382>.
- 413 (8) Yokelson, R. J.; Crouse, J. D.; DeCarlo, P. F.; Karl, T.; Urbanski, S.; Atlas, E.; Campos,  
414 T.; Shinozuka, Y.; Kapustin, V.; Clarke, A. D.; Weinheimer, A.; Knapp, D. J.; Montzka,  
415 D. D.; Holloway, J.; Weibring, P.; Flocke, F.; Zheng, W.; Toohey, D.; Wennberg, P. O.;  
416 Wiedinmyer, C.; Mauldin, L.; Fried, A.; Richter, D.; Walega, J.; Jimenez, J. L.; Adachi,  
417 K.; Buseck, P. R.; Hall, S. R.; Shetter, R. Emissions from Biomass Burning in the  
418 Yucatan. *Atmos. Chem. Phys.* **2009**, *9* (15), 5785–5812. [https://doi.org/10.5194/acp-9-](https://doi.org/10.5194/acp-9-5785-2009)  
419 [5785-2009](https://doi.org/10.5194/acp-9-5785-2009).
- 420 (9) Hennigan, C. J.; Sullivan, A. P.; Collett, J. L.; Robinson, A. L. Levoglucosan Stability in  
421 Biomass Burning Particles Exposed to Hydroxyl Radicals. *Geophys. Res. Lett.* **2010**, *37*  
422 (9), 1–4. <https://doi.org/10.1029/2010GL043088>.
- 423 (10) Hennigan, C. J.; Miracolo, M. A.; Engelhart, G. J.; May, A. A.; Presto, A. A.; Lee, T.;  
424 Sullivan, A. P.; McMeeking, G. R.; Coe, H.; Wold, C. E.; Hao, W. M.; Gilman, J. B.;  
425 Kuster, W. C.; De Gouw, J.; Schichtel, B. A.; Collett, J. L.; Kreidenweis, S. M.; Robinson,  
426 A. L. Chemical and Physical Transformations of Organic Aerosol from the Photo-  
427 Oxidation of Open Biomass Burning Emissions in an Environmental Chamber. *Atmos.*  
428 *Chem. Phys.* **2011**, *11* (15), 7669–7686. <https://doi.org/10.5194/acp-11-7669-2011>.
- 429 (11) Ortega, A. M.; Day, D. A.; Cubison, M. J.; Brune, W. H.; Bon, D.; De Gouw, J. A.;  
430 Jimenez, J. L. Secondary Organic Aerosol Formation and Primary Organic Aerosol  
431 Oxidation from Biomass-Burning Smoke in a Flow Reactor during FLAME-3. *Atmos.*  
432 *Chem. Phys.* **2013**, *13* (22), 11551–11571. <https://doi.org/10.5194/acp-13-11551-2013>.

- 433 (12) Bruns, E. A.; El Haddad, I.; Slowik, J. G.; Kilic, D.; Klein, F.; Baltensperger, U.; Prévôt,  
434 A. S. H. Identification of Significant Precursor Gases of Secondary Organic Aerosols  
435 from Residential Wood Combustion. *Sci. Rep.* **2016**, *6* (June), 1–9.  
436 <https://doi.org/10.1038/srep27881>.
- 437 (13) Bruns, E. A.; El Haddad, I.; Keller, A.; Klein, F.; Kumar, N. K.; Pieber, S. M.; Corbin, J.  
438 C.; Slowik, J. G.; Brune, W. H.; Baltensperger, U.; Prévôt, A. S. H. Inter-Comparison of  
439 Laboratory Smog Chamber and Flow Reactor Systems on Organic Aerosol Yield and  
440 Composition. *Atmos. Meas. Tech.* **2015**, *8* (6), 2315–2332. [https://doi.org/10.5194/amt-8-](https://doi.org/10.5194/amt-8-2315-2015)  
441 [2315-2015](https://doi.org/10.5194/amt-8-2315-2015).
- 442 (14) Jaffe, D. A.; Wigder, N. L. Ozone Production from Wildfires: A Critical Review. *Atmos.*  
443 *Environ.* **2012**, *51*, 1–10. <https://doi.org/http://dx.doi.org/10.1016/j.atmosenv.2011.11.063>.
- 444 (15) Brown, S. S.; Stutz, J. Nighttime Radical Observations and Chemistry. *Chem. Soc. Rev.*  
445 **2012**, *41*, 6405–6447. <https://doi.org/10.1039/c2cs35181a>.
- 446 (16) Wayne, R. .; Barnes, I.; Biggs, P.; Burrows, J. .; Canosa-Mas, C. .; Hjorth, J.; Le Bras, G.;  
447 Moortgat, G. .; Perner, D.; Poulet, G.; Restelli, G.; Sidebottom, H. The Nitrate Radical:  
448 Physics, Chemistry, and the Atmosphere. *Atmos. Environ. Part A. Gen. Top.* **1991**, *25* (1),  
449 1–203. [https://doi.org/10.1016/0960-1686\(91\)90192-A](https://doi.org/10.1016/0960-1686(91)90192-A).
- 450 (17) Osthoff, H. D.; Roberts, J. M.; Ravishankara, A. R.; Williams, E. J.; Lerner, B. M.;  
451 Sommariva, R.; Bates, T. S.; Coffman, D.; Quinn, P. K.; Dibb, J. E.; Stark, H.;  
452 Burkholder, J. B.; Talukdar, R. K.; Meagher, J.; Fehsenfeld, F. C.; Brown, S. S. High  
453 Levels of Nitryl Chloride in the Polluted Subtropical Marine Boundary Layer. *Nat.*  
454 *Geosci.* **2008**, *1* (5), 324–328. <https://doi.org/10.1038/ngeo177>.

- 455 (18) Thornton, J. A.; Kercher, J. P.; Riedel, T. P.; Wagner, N. L.; Cozic, J.; Holloway, J. S.;  
456 Dubé, W. P.; Wolfe, G. M.; Quinn, P. K.; Middlebrook, A. M.; Alexander, B.; Brown, S.  
457 S. A Large Atomic Chlorine Source Inferred from Mid-Continental Reactive Nitrogen  
458 Chemistry. *Nature* **2010**, *464* (7286), 271–274. <https://doi.org/10.1038/nature08905>.
- 459 (19) Chang, W. L.; Bhave, P. V.; Brown, S. S.; Riemer, N.; Stutz, J.; Dabdub, D.  
460 Heterogeneous Atmospheric Chemistry, Ambient Measurements, and Model Calculations  
461 of N<sub>2</sub>O<sub>5</sub>: A Review. *Aerosol Sci. Technol.* **2011**, *45* (6), 655–685.  
462 <https://doi.org/10.1080/02786826.2010.551672>.
- 463 (20) Ahern, A.; Goldberger, L.; Jahl, L.; Thornton, J.; Sullivan, R. C. Production of N<sub>2</sub>O<sub>5</sub> and  
464 ClNO<sub>2</sub> through Nocturnal Processing of Biomass-Burning Aerosol. *Environ. Sci. Technol.*  
465 **2018**, *52* (2), 550–559. <https://doi.org/10.1021/acs.est.7b04386>.
- 466 (21) Hatch, L. E.; Luo, W.; Pankow, J. F.; Yokelson, R. J.; Stockwell, C. E.; Barsanti, K. C.  
467 Identification and Quantification of Gaseous Organic Compounds Emitted from Biomass  
468 Burning Using Two-Dimensional Gas Chromatography–time-of-Flight Mass  
469 Spectrometry. *Atmos. Chem. Phys.* **2015**, *15* (4), 1865–1899. [https://doi.org/10.5194/acp-](https://doi.org/10.5194/acp-15-1865-2015)  
470 [15-1865-2015](https://doi.org/10.5194/acp-15-1865-2015).
- 471 (22) Stockwell, C. E.; Yokelson, R. J.; Kreidenweis, S. M.; Robinson, A. L.; Demott, P. J.;  
472 Sullivan, R. C.; Reardon, J.; Ryan, K. C.; Griffith, D. W. T.; Stevens, L. Trace Gas  
473 Emissions from Combustion of Peat, Crop Residue, Domestic Biofuels, Grasses, and  
474 Other Fuels: Configuration and Fourier Transform Infrared (FTIR) Component of the  
475 Fourth Fire Lab at Missoula Experiment (FLAME-4). *Atmos. Chem. Phys.* **2014**, *14* (18),  
476 9727–9754. <https://doi.org/10.5194/acp-14-9727-2014>.

- 477 (23) Selimovic, V.; Yokelson, R. J.; Warneke, C.; Roberts, J. M.; de Gouw, J. A.; Griffith, D.  
478 W. T. Aerosol Optical Properties and Trace Gas Emissions from Laboratory-Simulated  
479 Western US Wildfires during FIREX. *Atmos. Chem. Phys.* **2017**, *18*, 2929–2948.  
480 <https://doi.org/10.5194/acp-18-2929-2018>.
- 481 (24) Sekimoto, K.; Koss, A. R.; Gilman, J. B.; Selimovic, V.; Coggon, M. M.; Zarzana, K. J.;  
482 Yuan, B.; Lerner, B. M.; Brown, S. S.; Warneke, C.; Yokelson, R. J.; Roberts, J. M.; de  
483 Gouw, J. High- and Low-Temperature Pyrolysis Profiles Describe Volatile Organic  
484 Compound Emissions from Western US Wildfire Fuels. *Atmos. Chem. Phys. Discuss.*  
485 **2018**, No. February, 1–39. <https://doi.org/10.5194/acp-2018-52>.
- 486 (25) Hartikainen, A.; Yli-Pirilä, P.; Tiitta, P.; Leskinen, A.; Kortelainen, M.; Orasche, J.;  
487 Schnelle-Kreis, J.; Lehtinen, K.; Zimmermann, R.; Jokiniemi, J.; Sippula, O. Volatile  
488 Organic Compounds from Logwood Combustion: Emissions and Transformation under  
489 Dark and Photochemical Aging Conditions in a Smog Chamber. *Environ. Sci. Technol.*  
490 **2018**, *52* (4979–4988), [acs.est.7b06269](https://doi.org/10.1021/acs.est.7b06269). <https://doi.org/10.1021/acs.est.7b06269>.
- 491 (26) Atkinson, R.; Arey, J. Gas-Phase Tropospheric Chemistry of Biogenic Volatile Organic  
492 Compounds: A Review. In *Atmospheric Environment*; Pergamon, 2003; Vol. 37, pp 197–  
493 219. [https://doi.org/10.1016/S1352-2310\(03\)00391-1](https://doi.org/10.1016/S1352-2310(03)00391-1).
- 494 (27) Atkinson, R.; Arey, J. Atmospheric Degradation of Volatile Organic Compounds. *Chem.*  
495 *Rev.* **2003**, *103* (3), 4605–4638. <https://doi.org/10.1021/cr0206420>.
- 496 (28) Atkinson, R. Kinetics and Mechanisms of the Gas-Phase Reactions of the NO<sub>3</sub> Radical  
497 with Organic Compounds. *Journal of Physical and Chemical Reference Data*. 1991, pp  
498 459–507. <https://doi.org/10.1063/1.555887>.

- 499 (29) El Zein, A.; Coeur, C.; Obeid, E.; Lauraguais, A.; Fagniez, T. Reaction Kinetics of  
500 Catechol (1,2-Benzenediol) and Guaiacol (2-Methoxyphenol) with Ozone. *J. Phys. Chem.*  
501 *A* **2015**, *119* (26), 6759–6765. <https://doi.org/10.1021/acs.jpca.5b00174>.
- 502 (30) Martínez, E.; Cabañas, B.; Aranda, A.; Martín, P.; Salgado, S. Absolute Rate Coefficients  
503 for the Gas-Phase Reactions of NO<sub>3</sub> Radical with a Series of Monoterpenes at T = 298 to  
504 433 K. *J. Atmos. Chem.* **1999**, *33* (3), 265–282.  
505 <https://doi.org/10.1023/A:1006178530211>.
- 506 (31) Kerdouci, J.; Picquet-Varrault, B.; Doussin, J. F. Structure-Activity Relationship for the  
507 Gas-Phase Reactions of NO<sub>3</sub> radical with Organic Compounds: Update and Extension to  
508 Aldehydes. *Atmos. Environ.* **2014**, *84* (3), 363–372.  
509 <https://doi.org/10.1016/j.atmosenv.2013.11.024>.
- 510 (32) Grosjean, D.; Williams, E. L. Environmental Persistence of Organic Compounds  
511 Estimated from Structure-Reactivity and Linear Free-Energy Relationships. Unsaturated  
512 Aliphatics. *Atmos. Environ. Part A, Gen. Top.* **1992**, *26* (8), 1395–1405.  
513 [https://doi.org/10.1016/0960-1686\(92\)90124-4](https://doi.org/10.1016/0960-1686(92)90124-4).
- 514 (33) Cabañas, B.; Baeza, M. T.; Salgado, S.; Martín, P.; Taccone, R.; Martínez, E. Oxidation of  
515 Heterocycles in the Atmosphere: Kinetic Study of Their Reactions with NO<sub>3</sub> Radical. *J.*  
516 *Phys. Chem. A* **2004**, *108* (49), 10818–10823. <https://doi.org/10.1021/jp046524t>.
- 517 (34) Harrison, M. A. J.; Barra, S.; Borghesi, D.; Vione, D.; Arsene, C.; Iulian Olariu, R.  
518 Nitrated Phenols in the Atmosphere: A Review. *Atmospheric Environment*. 2005, pp 231–  
519 248. <https://doi.org/10.1016/j.atmosenv.2004.09.044>.
- 520 (35) Laskin, A.; Laskin, J.; Nizkorodov, S. A. Chemistry of Atmospheric Brown Carbon.

521 *Chem. Rev.* **2015**, *115* (10), 4335–4382. <https://doi.org/10.1021/cr5006167>.

522 (36) Zarzana, K. J.; Min, K. E.; Washenfelder, R. A.; Kaiser, J.; Krawiec-Thayer, M.; Peischl,  
523 J.; Neuman, J. A.; Nowak, J. B.; Wagner, N. L.; Dubè, W. P.; Clair, J. M. S.; Wolfe, G.  
524 M.; Hanisco, T. F.; Keutsch, F. N.; Ryerson, T. B.; Brown, S. S. Emissions of Glyoxal and  
525 Other Carbonyl Compounds from Agricultural Biomass Burning Plumes Sampled by  
526 Aircraft. *Environ. Sci. Technol.* **2017**, *51* (20), 11761–11770.  
527 <https://doi.org/10.1021/acs.est.7b03517>.

528 (37) Neuman, J. A.; Trainer, M.; Brown, S. S.; Min, K. E.; Nowak, J. B.; Parrish, D. D.;  
529 Peischl, J.; Pollack, I. B.; Roberts, J. M.; Ryerson, T. B.; Veres, P. R. HONO Emission  
530 and Production Determined from Airborne Measurements over the Southeast U.S. *J.*  
531 *Geophys. Res.* **2016**, *121* (15), 9237–9250. <https://doi.org/10.1002/2016JD025197>.

532 (38) Warneke, C.; Trainer, M.; De Gouw, J. A.; Parrish, D. D.; Fahey, D. W.; Ravishankara, A.  
533 R.; Middlebrook, A. M.; Brock, C. A.; Roberts, J. M.; Brown, S. S.; Neuman, J. A.;  
534 Lerner, B. M.; Lack, D.; Law, D.; Hübler, G.; Pollack, I.; Sjostedt, S.; Ryerson, T. B.;  
535 Gilman, J. B.; Liao, J.; Holloway, J.; Peischl, J.; Nowak, J. B.; Aikin, K. C.; Min, K. E.;  
536 Washenfelder, R. A.; Graus, M. G.; Richardson, M.; Markovic, M. Z.; Wagner, N. L.;  
537 Welti, A.; Veres, P. R.; Edwards, P.; Schwarz, J. P.; Gordon, T.; Dube, W. P.; McKeen, S.  
538 A.; Brioude, J.; Ahmadov, R.; Bougiatioti, A.; Lin, J. J.; Nenes, A.; Wolfe, G. M.;  
539 Hanisco, T. F.; Lee, B. H.; Lopez-Hilfiker, F. D.; Thornton, J. A.; Keutsch, F. N.; Kaiser,  
540 J.; Mao, J.; Hatch, C. D. Instrumentation and Measurement Strategy for the NOAA  
541 SENEX Aircraft Campaign as Part of the Southeast Atmosphere Study 2013. *Atmos.*  
542 *Meas. Tech.* **2016**, *9* (7), 3063–3093. <https://doi.org/10.5194/amt-9-3063-2016>.

- 543 (39) Brown, S. S.; Stark, H.; Ravishankara, A. R. Cavity Ring-down Spectroscopy for  
544 Atmospheric Trace Gas Detection: Application to the Nitrate Radical (NO<sub>3</sub>). *Appl. Phys.*  
545 *B Lasers Opt.* **2002**, *75* (2–3), 173–182. <https://doi.org/10.1007/s00340-002-0980-y>.
- 546 (40) Dubé, W. P.; Brown, S. S.; Osthoff, H. D.; Nunley, M. R.; Ciciora, S. J.; Paris, M. W.;  
547 McLaughlin, R. J.; Ravishankara, A. R. Aircraft Instrument for Simultaneous, *in Situ*  
548 Measurement of NO<sub>3</sub> and N<sub>2</sub>O<sub>5</sub> via Pulsed Cavity Ring-down Spectroscopy. *Rev. Sci.*  
549 *Instrum.* **2006**, *77* (3), 034101. <https://doi.org/10.1063/1.2176058>.
- 550 (41) Fuchs, H.; Dubé, W. P.; Ciciora, S. J.; Brown, S. S. Determination of Inlet Transmission  
551 and Conversion Efficiencies for *in Situ* Measurements of the Nocturnal Nitrogen Oxides,  
552 NO<sub>3</sub>, N<sub>2</sub>O<sub>5</sub> and NO<sub>2</sub>, via Pulsed Cavity Ring-down Spectroscopy. *Anal. Chem.* **2008**, *80*  
553 (15), 6010–6017. <https://doi.org/10.1021/ac8007253>.
- 554 (42) Wild, R. J.; Edwards, P. M.; Dube, W. P.; Baumann, K.; Edgerton, E. S.; Quinn, P. K.;  
555 Roberts, J. M.; Rollins, A. W.; Veres, P. R.; Warneke, C.; Williams, E. J.; Yuan, B.;  
556 Brown, S. S.; Dubé, W. P.; Baumann, K.; Edgerton, E. S.; Quinn, P. K.; Roberts, J. M.;  
557 Rollins, A. W.; Veres, P. R.; Warneke, C.; Williams, E. J.; Yuan, B.; Brown, S. S. A  
558 Measurement of Total Reactive Nitrogen, NO<sub>y</sub>, Together with NO<sub>2</sub>, NO, and O<sub>3</sub> via  
559 Cavity Ring-down Spectroscopy. *Environ. Sci. Technol.* **2014**, *48* (16), 9609–9615.  
560 <https://doi.org/10.1021/es501896w>.
- 561 (43) Ryerson, T. B.; Huey, L. G.; Knapp, K.; Nueman, J. A.; Parrish, D. D.; Sueper, D. T.;  
562 Fehsenfeld, F. C. Design and Initial Characterization of an Inlet for Gas-Phase NO<sub>y</sub>  
563 Measurements from Aircraft. *J. Geophys. Res. Atmos.* **1999**, *104* (D5), 5483–5492.
- 564 (44) Brock, C. A.; Schröder, F.; Kärcher, B.; Petzold, A.; Busen, R.; Fiebig, M. Ultrafine

565 Particle Size Distribution Measured in Aircraft Exhaust Plumes. *J. Geophys. Res.* **2000**,  
566 *105* (Vi), 26555–26567.

567 (45) Brock, C. A.; Cozic, J.; Bahreini, R.; Froyd, K. D.; Middlebrook, A. M.; McComiskey,  
568 A.; Brioude, J.; Cooper, O. R.; Stohl, A.; Aikin, K. C.; De Gouw, J. A.; Fahey, D. W.;  
569 Ferrare, R. A.; Gao, R. S.; Gore, W.; Holloway, J. S.; Hübler, G.; Jefferson, A.; Lack, D.  
570 A.; Lance, S.; Moore, R. H.; Murphy, D. M.; Nenes, A.; Novelli, P. C.; Nowak, J. B.;  
571 Ogren, J. A.; Peischl, J.; Pierce, R. B.; Pilewskie, P.; Quinn, P. K.; Ryerson, T. B.;  
572 Schmidt, K. S.; Schwarz, J. P.; Sodemann, H.; Spackman, J. R.; Stark, H.; Thomson, D.  
573 S.; Thornberry, T.; Veres, P.; Watts, L. A.; Warneke, C.; Wollny, A. G. Characteristics,  
574 Sources, and Transport of Aerosols Measured in Spring 2008 during the Aerosol,  
575 Radiation, and Cloud Processes Affecting Arctic Climate (ARCPAC) Project. *Atmos.*  
576 *Chem. Phys.* **2011**, *11* (6), 2423–2453. <https://doi.org/10.5194/acp-11-2423-2011>.

577 (46) De Gouw, J.; Warneke, C. Measurements of Volatile Organic Compounds in the Earth's  
578 Atmosphere Using Proton-Transfer-Reaction Mass Spectrometry. *Mass Spectrometry*  
579 *Reviews*. Wiley-Blackwell March 1, 2007, pp 223–257.  
580 <https://doi.org/10.1002/mas.20119>.

581 (47) Bond, T. C.; Doherty, S. J.; Fahey, D. W.; Forster, P. M.; Berntsen, T.; Deangelo, B. J.;  
582 Flanner, M. G.; Ghan, S.; Kärcher, B.; Koch, D.; Kinne, S.; Kondo, Y.; Quinn, P. K.;  
583 Sarofim, M. C.; Schultz, M. G.; Schulz, M.; Venkataraman, C.; Zhang, H.; Zhang, S.;  
584 Bellouin, N.; Guttikunda, S. K.; Hopke, P. K.; Jacobson, M. Z.; Kaiser, J. W.; Klimont,  
585 Z.; Lohmann, U.; Schwarz, J. P.; Shindell, D.; Storelvmo, T.; Warren, S. G.; Zender, C. S.  
586 Bounding the Role of Black Carbon in the Climate System: A Scientific Assessment. *J.*  
587 *Geophys. Res. Atmos.* **2013**, *118* (11), 5380–5552. <https://doi.org/10.1002/jgrd.50171>.

- 588 (48) Min, K.-E.; Washenfelder, R. a.; Dubé, W. P.; Langford, a. O.; Edwards, P. M.; Zarzana,  
589 K. J.; Stutz, J.; Lu, K.; Rohrer, F.; Zhang, Y.; Brown, S. S. A Broadband Cavity Enhanced  
590 Absorption Spectrometer for Aircraft Measurements of Glyoxal, Methylglyoxal, Nitrous  
591 Acid, Nitrogen Dioxide, and Water Vapor. *Atmos. Meas. Tech. Discuss.* **2016**, *9* (10),  
592 423–440. <https://doi.org/10.5194/amtd-8-11209-2015>.
- 593 (49) Zheng, W.; Flocke, F. M.; Tyndall, G. S.; Swanson, A.; Orlando, J. J.; Roberts, J. M.;  
594 Huey, L. G.; Tanner, D. J. Characterization of a Thermal Decomposition Chemical  
595 Ionization Mass Spectrometer for the Measurement of Peroxy Acyl Nitrates (PANs) in the  
596 Atmosphere. *Atmos. Chem. Phys.* **2011**, *11* (13), 6529–6547. [https://doi.org/10.5194/acp-](https://doi.org/10.5194/acp-11-6529-2011)  
597 [11-6529-2011](https://doi.org/10.5194/acp-11-6529-2011).
- 598 (50) Schwarz, J. P.; Gao, R. S.; Fahey, D. W.; Thomson, D. S.; Watts, L. A.; Wilson, J. C.;  
599 Reeves, J. M.; Darbeheshti, M.; Baumgardner, D. G.; Kok, G. L.; Chung, S. H.; Schulz,  
600 M.; Hendricks, J.; Lauer, A.; Kärcher, B.; Slowik, J. G.; Rosenlof, K. H.; Thompson, T.  
601 L.; Langford, A. O.; Loewenstein, M.; Aikin, K. C. Single-Particle Measurements of  
602 Midlatitude Black Carbon and Light-Scattering Aerosols from the Boundary Layer to the  
603 Lower Stratosphere. *J. Geophys. Res. Atmos.* **2006**, *111* (16), 1–15.  
604 <https://doi.org/10.1029/2006JD007076>.
- 605 (51) Holloway, J. S.; Jakoubek, R. O.; Parrish, D. D.; Gerbig, C.; Volz-Thomas, A.;  
606 Schmitgen, S.; Fried, A.; Wert, B.; Henry, B.; Drummond, J. R. Airborne Intercomparison  
607 of Vacuum Ultraviolet Fluorescence and Tunable Diode Laser Absorption Measurements  
608 of Tropospheric Carbon Monoxide. *J. Geophys. Res. Atmos.* **2000**, *105* (D19), 24251–  
609 24261. <https://doi.org/10.1029/2000JD900237>.

- 610 (52) Stockwell, C. E.; Veres, P. R.; Williams, J.; Yokelson, R. J. Characterization of Biomass  
611 Burning Emissions from Cooking Fires, Peat, Crop Residue, and Other Fuels with High-  
612 Resolution Proton-Transfer-Reaction Time-of-Flight Mass Spectrometry. *Atmos. Chem.*  
613 *Phys.* **2015**, *15* (2), 845–865. <https://doi.org/10.5194/acp-15-845-2015>.
- 614 (53) Kerdouci, J.; Picquet-Varrault, B.; Doussin, J. F. Prediction of Rate Constants for Gas-  
615 Phase Reactions of Nitrate Radical with Organic Compounds: A New Structure-Activity  
616 Relationship. *ChemPhysChem* **2010**, *11* (18), 3909–3920.  
617 <https://doi.org/10.1002/cphc.201000673>.
- 618 (54) Edwards, P. M.; Aikin, K. C.; Dube, W. P.; Fry, J. L.; Gilman, J. B.; De Gouw, J. A.;  
619 Graus, M. G.; Hanisco, T. F.; Holloway, J.; Hübler, G.; Kaiser, J.; Keutsch, F. N.; Lerner,  
620 B. M.; Neuman, J. A.; Parrish, D. D.; Peischl, J.; Pollack, I. B.; Ravishankara, A. R.;  
621 Roberts, J. M.; Ryerson, T. B.; Trainer, M.; Veres, P. R.; Wolfe, G. M.; Warneke, C.  
622 Transition from High- to Low-NO<sub>x</sub> Control of Night-Time Oxidation in the Southeastern  
623 US. *Nat. Geosci.* **2017**, *10* (7), 490–495. <https://doi.org/10.1038/ngeo2976>.
- 624 (55) Wolfe, G. M.; Marvin, M. R.; Roberts, S. J.; Travis, K. R.; Liao, J. The Framework for 0-  
625 D Atmospheric Modeling (F0AM) v3.1. *Geosci. Model Dev.* **2016**, *9* (9), 3309–3319.  
626 <https://doi.org/10.5194/gmd-9-3309-2016>.
- 627 (56) Jenkin, M. E.; Saunders, S. M.; Pilling, M. J. The Tropospheric Degradation of Volatile  
628 Organic Compounds: A Protocol for Mechanism Development. *Atmos. Environ.* **1997**, *31*  
629 (1), 81–104. [https://doi.org/10.1016/S1352-2310\(96\)00105-7](https://doi.org/10.1016/S1352-2310(96)00105-7).
- 630 (57) Jenkin, M. E.; Saunders, S. M.; Wagner, V.; Pilling, M. J. Protocol for the Development  
631 of the Master Chemical Mechanism, MCM v3 (Part B): Tropospheric Degradation of

- 632 Aromatic Volatile Organic Compounds. *Atmos. Chem. Phys.* **2003**, *3* (1), 181–193.  
633 <https://doi.org/10.5194/acp-3-181-2003>.
- 634 (58) Bloss, C.; Wagner, V.; Jenkin, M. E.; Volkamer, R.; Bloss, W. J.; Lee, J. D.; Heard, D. E.;  
635 Wirtz, K.; Martin-Reviejo, M.; Rea, G.; Wenger, J. C.; Pilling, M. J. Development of a  
636 Detailed Chemical Mechanism (MCMv3.1) for the Atmospheric Oxidation of Aromatic  
637 Hydrocarbons. *Atmos. Chem. Phys.* **2005**, *5* (3), 641–664. [https://doi.org/10.5194/acp-5-](https://doi.org/10.5194/acp-5-641-2005)  
638 [641-2005](https://doi.org/10.5194/acp-5-641-2005).
- 639 (59) Jenkin, M. E.; Wyche, K. P.; Evans, C. J.; Carr, T.; Monks, P. S.; Alfarra, M. R.; Barley,  
640 M. H.; McFiggans, G. B.; Young, J. C.; Rickard, A. R. Development and Chamber  
641 Evaluation of the MCM v3.2 Degradation Scheme for  $\beta$ -Caryophyllene. *Atmos. Chem.*  
642 *Phys.* **2012**, *12* (11), 5275–5308. <https://doi.org/10.5194/acp-12-5275-2012>.
- 643 (60) Jenkin, M. E.; Young, J. C.; Rickard, A. R. The MCM v3.3.1 Degradation Scheme for  
644 Isoprene. *Atmos. Chem. Phys.* **2015**, *15* (20), 11433–11459. [https://doi.org/10.5194/acp-](https://doi.org/10.5194/acp-15-11433-2015)  
645 [15-11433-2015](https://doi.org/10.5194/acp-15-11433-2015).
- 646 (61) Yang, B.; Zhang, H.; Wang, Y.; Zhang, P.; Shu, J.; Sun, W.; Ma, P. Experimental and  
647 Theoretical Studies on Gas-Phase Reactions of NO<sub>3</sub> Radicals with Three  
648 Methoxyphenols: Guaiacol, Creosol, and Syringol. *Atmos. Environ.* **2016**, *125* (3), 243–  
649 251. <https://doi.org/10.1016/j.atmosenv.2015.11.028>.
- 650 (62) Tapia, A.; Villanueva, F.; Salgado, M. S.; Cabañas, B.; Martínez, E.; Martín, P.  
651 Atmospheric Degradation of 3-Methylfuran: Kinetic and Products Study. *Atmos. Chem.*  
652 *Phys.* **2011**, *11* (7), 3227–3241. <https://doi.org/10.5194/acp-11-3227-2011>.
- 653 (63) Lauraguais, A.; El Zein, A.; Coeur, C.; Obeid, E.; Cassez, A.; Rayez, M.-T.; Rayez, J.-C.

- 654 Kinetic Study of the Gas-Phase Reactions of Nitrate Radicals with Methoxyphenol  
655 Compounds: Experimental and Theoretical Approaches. *J. Phys. Chem. A* **2016**, *120* (17),  
656 2691–2699. <https://doi.org/10.1021/acs.jpca.6b02729>.
- 657 (64) CropScape - NASS CDL Program <https://nassgeodata.gmu.edu/CropScape/> (accessed Aug  
658 6, 2018).
- 659 (65) Brown, S. Absorption Spectroscopy in High Finesse Cavities for Atmospheric Studies.  
660 *Chem. Rev.* **2003**, *103*, 5219.
- 661 (66) Brown, S. S.; Stark, H.; Ravishankara, A. R. Applicability of the Steady State  
662 Approximation to the Interpretation of Atmospheric Observations of NO<sub>3</sub> and N<sub>2</sub>O<sub>5</sub>. *J.*  
663 *Geophys. Res.* **2003**, *108* (D17), 4539. <https://doi.org/10.1029/2003JD003407>.
- 664 (67) Olariu, R. I.; Bejan, I.; Barnes, I.; Klotz, B.; Becker, K. H.; Wirtz, K. Rate Coefficients for  
665 the Gas-Phase Reaction of NO<sub>3</sub> Radicals with Selected Dihydroxybenzenes. *Int. J. Chem.*  
666 *Kinet.* **2004**, *36* (11), 577–583. <https://doi.org/10.1002/kin.20029>.
- 667 (68) Finewax, Z.; De Gouw, J. A.; Ziemann, P. J. Identification and Quantification of 4-  
668 Nitrocatechol Formed from OH and NO<sub>3</sub> Radical-Initiated Reactions of Catechol in Air in  
669 the Presence of NO<sub>x</sub>: Implications for Secondary Organic Aerosol Formation from  
670 Biomass Burning. *Environ. Sci. Technol.* **2018**, *52* (4), 1981–1989.  
671 <https://doi.org/10.1021/acs.est.7b05864>.
- 672 (69) Desyaterik, Y.; Sun, Y.; Shen, X.; Lee, T.; Wang, X.; Wang, T.; Collett, J. L. Speciation  
673 of “Brown” Carbon in Cloud Water Impacted by Agricultural Biomass Burning in Eastern  
674 China. *J. Geophys. Res. Atmos.* **2013**, *118* (13), 7389–7399.  
675 <https://doi.org/10.1002/jgrd.50561>.

- 676 (70) Claeys, M.; Vermeylen, R.; Yasmeen, F.; Gómez-González, Y.; Chi, X.; Maenhaut, W.;  
677 Mészáros, T.; Salma, I. Chemical Characterisation of Humic-like Substances from Urban,  
678 Rural and Tropical Biomass Burning Environments Using Liquid Chromatography with  
679 UV/Vis Photodiode Array Detection and Electrospray Ionisation Mass Spectrometry.  
680 *Environ. Chem.* **2012**, *9* (3), 273–284. <https://doi.org/10.1071/EN11163>.
- 681 (71) Lin, P.; Bluvshstein, N.; Rudich, Y.; Nizkorodov, S. A.; Laskin, J.; Laskin, A. Molecular  
682 Chemistry of Atmospheric Brown Carbon Inferred from a Nationwide Biomass Burning  
683 Event. *Environ. Sci. Technol.* **2017**, *51* (20), 11561–11570.  
684 <https://doi.org/10.1021/acs.est.7b02276>.
- 685 (72) Iinuma, Y.; Boge, O.; Grade, R.; Herrmann, H. Methyl-Nitrocatechols : Atmospheric  
686 Tracer Compounds for Biomass Burning Secondary Organic Aerosols. *Environ. Sci.*  
687 *Technol.* **2010**, *44*, 8453–8459.
- 688 (73) Gaston, C. J.; Lopez-Hilfiker, F. D.; Whybrew, L. E.; Hadley, O.; McNair, F.; Gao, H.;  
689 Jaffe, D. A.; Thornton, J. A. Online Molecular Characterization of Fine Particulate Matter  
690 in Port Angeles, WA: Evidence for a Major Impact from Residential Wood Smoke.  
691 *Atmos. Environ.* **2016**, *138*, 99–107. <https://doi.org/10.1016/j.atmosenv.2016.05.013>.
- 692 (74) Mohr, C.; Lopez-Hilfiker, F. D.; Zotter, P.; Prévôt, A. S. H.; Xu, L.; Ng, N. L.; Herndon,  
693 S. C.; Williams, L. R.; Franklin, J. P.; Zahniser, M. S.; Worsnop, D. R.; Knighton, W. B.;  
694 Aiken, A. C.; Gorkowski, K. J.; Dubey, M. K.; Allan, J. D.; Thornton, J. A. Contribution  
695 of Nitrated Phenols to Wood Burning Brown Carbon Light Absorption in Detling, United  
696 Kingdom during Winter Time. *Environ. Sci. Technol.* **2013**, *47* (12), 6316–6324.  
697 <https://doi.org/10.1021/es400683v>.

- 698 (75) Xie, M.; Chen, X.; Hays, M. D.; Lewandowski, M.; Offenberg, J.; Kleindienst, T. E.;  
699 Holder, A. L. Light Absorption of Secondary Organic Aerosol: Composition and  
700 Contribution of Nitroaromatic Compounds. *Environ. Sci. Technol.* **2017**, *51* (20), 11607–  
701 11616. <https://doi.org/10.1021/acs.est.7b03263>.
- 702 (76) Hinrichs, R. Z.; Buczek, P.; Trivedi, J. J. Solar Absorption by Aerosol-Bound  
703 Nitrophenols Compared to Aqueous and Gaseous Nitrophenols. *Environ. Sci. Technol.*  
704 **2016**, *50* (11), 5661–5667. <https://doi.org/10.1021/acs.est.6b00302>.
- 705 (77) Odum Jay, R.; Hoffmann, T.; Bowman, F.; Collins, D.; Flagan Richard, C.; Seinfeld John,  
706 H. Gas Particle Partitioning and Secondary Organic Aerosol Yields. *Environ. Sci.*  
707 *Technol.* **1996**, *30* (8), 2580–2585. <https://doi.org/10.1021/es950943+>.
- 708